Materials Today Bio 26 (2024) 101073

Contents lists available at ScienceDirect

Materials Today Bio

journal homepage: www.journals.elsevier.com/materials-today-bio

A recombinant chimeric spider pyriform-aciniform silk with highly tunable mechanical performance

Anupama Ghimire [a], Lingling Xu [a], Xiang-Qin Liu [a], Jan K. Rainey [a,b,c,*]

[a] Department of Biochemistry & Molecular Biology, Dalhousie University, Halifax, NS, B3H 4R2, Canada
[b] Department of Chemistry, Dalhousie University, Halifax, NS, B3H 4R2, Canada
[c] School of Biomedical Engineering, Dalhousie University, Halifax, NS, B3H 4R2, Canada

ARTICLE INFO

Keywords:
Pyriform (piriform) silk
Aciniform (wrapping) silk
Protein engineering
Biomaterials
Wet-spinning

ABSTRACT

Spider silks are natural protein-based biomaterials which are renowned for their mechanical properties and hold great promise for applications ranging from high-performance textiles to regenerative medicine. While some spiders can produce several different types of silks, most spider silk types – including pyriform and aciniform silks – are relatively unstudied. Pyriform and aciniform silks have distinct mechanical behavior and physicochemical properties, with materials produced using combinations of these silks currently unexplored. Here, we introduce an engineered chimeric fusion protein consisting of two repeat units of pyriform (Py) silk followed by two repeat units of aciniform (W) silk named Py_2W_2. This recombinant ~86.5 kDa protein is amenable to expression and purification from *Escherichia coli* and exhibits high α-helicity in a fluorinated acid- and alcohol-based solution used to form a dope for wet-spinning. Wet-spinning enables continuous fiber production and post-spin stretching of the wet-spun fibers in air or following submersion in water or ethanol leads to increases in optical anisotropy, consistent with increased molecular alignment along the fiber axis. Mechanical properties of the fibers vary as a function of post-spin stretching condition, with the highest extensibility and strength observed in air-stretched and ethanol-treated fibers, respectively, with mechanics being superior to fibers spun from either constituent protein alone. Notably, the maximum extensibility obtained (~157 ± 38 %) is of the same magnitude reported for natural flagelliform silks, the class of spider silk most associated with being stretchable. Interestingly, Py_2W_2 is also water-compatible, unlike its constituent Py_2. Fiber-state secondary structure correlates well with the observed mechanical properties, with depleted α-helicity and increased β-sheet content in cases of increased strength. Py_2W_2 fibers thus provide enhanced materials behavior in terms of their mechanics, tunability, and fiber properties, providing new directions for design and development of biomaterials suitable and tunable for disparate applications.

1. Introduction

Spiders are masters in making silks, which are composed of proteins called spidroins. Some spider species produce seven different types of silk, supporting various biological functions including locomotion, wrapping of prey, web construction, and protection of eggs, alongside others [1]. Corresponding to this functional variability, spider silks have diverse and incredible mechanical properties, with some being stronger than steel, tougher than Kevlar, or more flexible than nylon, with strength or toughness being considered on a per weight basis [2]. The functional versatility of spider silk proteins, along with their biocompatibility and biodegradability, has led to the fabrication of spider silk-based biomaterials with different structures, including fibers [3–6], films [7–9], hydrogels [10], and nanoparticles [11], with potential applications in controlled drug delivery [12], sutures [13], artificial ligaments [14], and others [15,16]. Corresponding to this outstanding potential for utility in diverse applications, recombinant silk proteins and fiber spinning methods continue to be actively developed (e.g., Refs. [17–19]).

Typically, spidroins have an architecture consisting of relatively short non-repetitive N- and C-terminal domains surrounding a much longer central repetitive domain (Fig. 1a). Because it constitutes the major portion of a given spidroin, the central repetitive domain is typically held responsible for the mechanical properties of the silk [20]. The current understanding of spider silk structure-function relationships

* Corresponding author. Department of Biochemistry & Molecular Biology, Dalhousie University, 5850 College Street Room 9B, PO Box 15000, Halifax, NS, B3H 4R2, Canada.
E-mail address: jan.rainey@dal.ca (J.K. Rainey).

https://doi.org/10.1016/j.mtbio.2024.101073
Received 31 January 2024; Received in revised form 11 April 2024; Accepted 25 April 2024
Available online 27 April 2024
2590-0064/© 2024 The Authors. Published by Elsevier Ltd. This is an open access article under the CC BY-NC license (http://creativecommons.org/licenses/by-nc/4.0/).

Abbreviations

AcSp1 – aciniform spidroin 1
AS – as-spun
ATR – attenuated total reflectance
CD – circular dichroism
EtOH – ethanol
Flag – flagelliform silk
$Flag_R$-$AcSp1_R$ – fused protein comprising Flag repetitive domain and AcSp1 repetitive domain
FTIR – Fourier transform infrared
LB – Luria-Bertani
MA – major ampullate
Py – repeat unit of PySp1 from *Argiope argentata*
Py_n – tandem repeat protein comprising n Py units
PySp1 – pyriform spidroin 1
SDS-PAGE – sodium dodecyl sulfate-polyacrylamide gel electrophoresis
SEM – scanning electron microscopy
TEM – transmission electron microscopy
TFA – trifluoroacetic acid
TFE – 2,2,2-trifluoroethanol
UV – ultraviolet
W – repeat unit of AcSp1 from *Argiope trifasciata*
W_2C_{ma2} – fused protein comprising two W units and a non-repetitive MA (MaSp2) C-terminal domain
W_n – tandem repeat protein comprising n W units
$Y1S8_{20}$ – fused protein comprising Flag and MA (specifically, MaSp2) repetitive domains

is predominantly based on dragline (major ampullate, MA) silk [21,22], which is the most extensively studied type of spider silk. The repetitive domain of MA spidroins consists of short motifs such as $(GA)_n$, $(GGX)_n$, $(A)_n$ and $(GPGXX)_n$, which are repeated many times and which have been directly associated with the mechanical properties of MA silk fibers [20,23]. Namely, poly-Ala stretches are associated with crystalline β-sheet domains that are responsible for the strength of the fibers, whereas GPG motifs likely fold into type II β-turns which contribute to extensibility. However, these short motifs are absent in several other spider silks, including the aciniform and pyriform silks that we focus on here.

Aciniform silk is composed of the protein aciniform spidroin 1 (AcSp1) and is primarily used to wrap and immobilize prey [24]. The central repetitive domain of AcSp1 from *Argiope trifasciata* consists of 14 or more 200 amino acid-long repeat ("W") units [24]. The W unit lacks short motifs, although it does contain an S-rich region. In comparison, pyriform silk is composed of pyriform spidroin 1 (PySp1) and is the fibrous component of a composite material used to form junctions that connect different silk types together and to attach web fibers to substrates [25]. The central repetitive domain of PySp1 from *Argiope argentata* consists of 21 repeat ("Py") units, each containing 234 amino acids [26]. The Py unit contains distinctive QSXXXQ motifs near the N-terminal end and an XP-rich motif near the C-terminal end [26]. The amino acid compositions of the W and Py are dissimilar, with the biggest distinctions being a high prevalence of Gly in W vs. Gln in Py (Fig. 1b).

A variety of recombinant W unit-based proteins capable of forming fibers have now been produced, ranging in size from W_2 to W_4 (i.e., tandem repeat proteins with two or four W units from *A. trifasciata*), with both hand-drawing [4,5,27,28] and wet-spinning [4,29] approaches developed and applied to produce fibers. Wet-spinning of Py_2 (a tandem repeat of two Py units from *A. argentata*) has also been performed [3]. Fibers formed from recombinant W unit and Py unit constructs show distinct properties. W unit-based fibers typically exhibit a combination of relatively high extensibility (e.g., ~20–40 %) and a molecular weight-dependent strength [4,29], features that combine to provide relatively tough fibers that are also amenable to stretching in water. Mechanics of Py_2-based fibers were observed to be more readily tunable than W-based fibers through relatively modest changes in post-spin stretching conditions, but fibers wet-spun from this protein construct are not amenable to post-spin stretching in water [3]. Both the W unit and Py unit exhibit mixed α-helical and disordered secondary structure in the solution-state [27,30], with partial loss of α-helical content and appearance of β-sheet structuring in the fiber states of both recombinant spidroins [3,27]. These structural transformations, including a retention of α-helical character in the fibrous states, are akin to those observed in natural aciniform and pyriform silks [31].

Several studies have shown enhanced properties relative to the constituent spidroins through fusion of motifs or modules from different

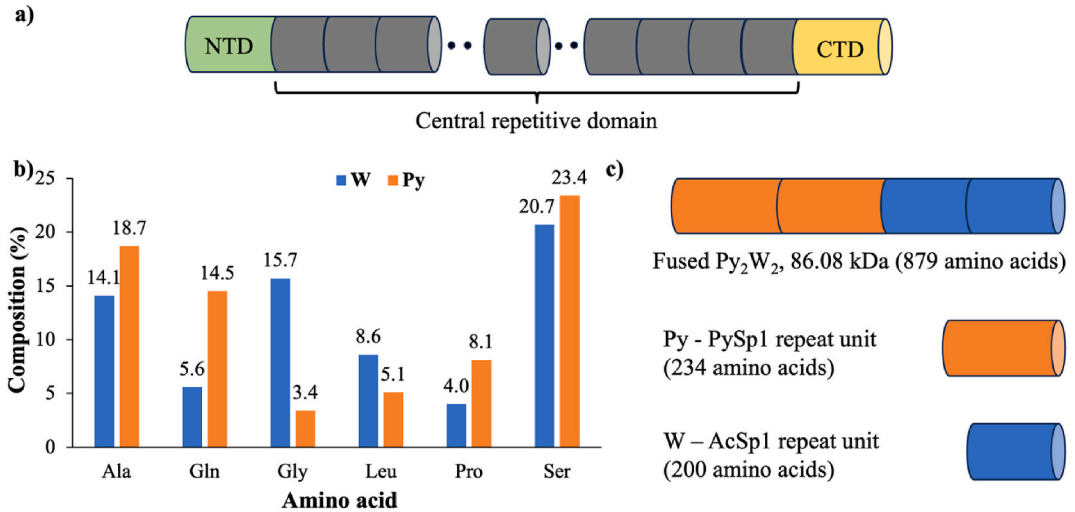

Fig. 1. a) Schematic representation of typical spider silk protein architecture, with a length central repetitive domain flanked by non-repetitive N- and C- terminal domains. b) Most prevalent amino acids of *Argiope trifasciata* aciniform silk repetitive unit (W) and *Argiope argentata* pyriform silk repetitive unit (Py). c) Schematic representation of chimeric fused Py_2W_2 protein (full sequence in Fig. S1).

spidroins to obtain new chimeric protein-based biomaterials. These have predominantly involved motifs of either MA or flagelliform (Flag) silk. Chimeric spidroins of fused W_2 and C-terminal domains of MA (W_2C_{ma2}) [28], fused motifs from Flag and MA silk [32], and fused repetitive modules from Flag and aciniform silk ($Flag_R$-$AcSp1_R$) [33] all resulted in fibers with superior mechanical properties relative to fibers spun with individual spidroins. For example, the average breaking strength of W_2Cma_2 fibers was 135.3 ± 36.6 MPa, significantly higher than those of W_2 (66.7 ± 15.8 MPa) [28].

Both the W unit and Py unit provide distinct potential for rational protein engineering given that both have lengthy disordered segments in the tandem repeat unit [27,30,34] and a lack of short motifs. Theis enables amino acid substitution, protein sequence insertion, or conjugation reactions in a manner less deleterious to fiber formation than would be the case in a spidroin such as MA with many short motifs directly associated with functional performance. Precedents of enhanced materials performance from other hybrid silks thus provide strong incentive to investigate the potential of aciniform-pyriform hybrid silks.

To evaluate the potential to synergistically combine properties of aciniform and pyriform silks, we engineered the chimeric protein Py_2W_2 comprising modules from both aciniform and pyriform silks (i.e., a fusion protein with two repeat units from each spidroin, Fig. 1c and S1). Using *Escherichia coli,* the ~86.5 kDa recombinant Py_2W_2 protein was readily produced by shake flask culturing at good yield (>230 mg of pure protein per L of *E. coli* culture). Py_2W_2 fibers were readily formed by wet-spinning and subjected to various post-spin stretching conditions, with changes in fiber-state secondary structure evaluated using Fourier transform infrared (FTIR) spectromicroscopy. Fiber morphology was analyzed by light and electron microscopy and mechanics were determined using stress-strain testing. Both surface morphology and mechanical behavior of Py_2W_2 fibers were dependent on post-spin stretching conditions, with some conditions providing extremely extensible fibers and others providing less extensible but stronger fibers with similar toughness. The mechanical tuneability of Py_2W_2 would be highly useful for downstream application, with potential to substantially exceed the extensibility observed for either of the parent recombinant silk proteins or for the corresponding natural spider silks.

2. Methods

2.1. Recombinant protein design, expression, and purification

To construct the expression plasmid, PCR-amplified DNA encoding for Py_2 and W_2 was fused and inserted into a modified pET32 vector using the same cloning strategy as described in previous study [5]. The open reading frame also encoded for an N-terminal His_6-tag, with full protein sequence provided in Fig. S1. Chemically competent BL21(DE3) *E. coli* cells were transformed with the Py_2W_2-encoding plasmid and an isolated single colony from an agar plate was used to inoculate a starter culture in Luria-Bertani (LB) medium containing 50 μg/mL of ampicillin. In brief, a starter culture was added to 1.2 L LB medium at 1:50 (v:v) and allowed to grow at 37 °C until the optical density measured at 600 nm reached between 0.9 and 1.2. The cells were then pelleted and transferred to M9 medium supplemented with a cocktail of amino acids (Table S1) [35]. Overexpression of Py_2W_2 was induced by adding 0.8 mM of iso-propyl-β-D-1-thiogalactopyranoside followed by incubation with shaking for 20 h at 20 °C. The cells were harvested and resuspended in native lysis buffer (50 mM NaH_2PO_4, 300 mM NaCl, 10 mM imidazole, pH 8.0) and lysed via French Pressure Cell (American Instrument Company, Silver Spring, MD; equipped with a pressure cell from Glen Mills Inc., Clifton, NJ). The cell lysate was centrifuged at 12000 rcf for 30 min at 4 °C and the resulting pellets were resuspended in denaturing buffer (100 mM NaH_2PO_4, 10 mM Tris-base, 8 M urea, pH 8), and the supernatant was passed through a nickel affinity column (Ni SuperFlow Resin, Takara Bio, San Jose, CA). Py_2W_2 was eluted with elution buffer (100 mM NaH_2PO_4, 10 mM Tris-base, 4 M urea, 250 mM imidazole, pH 8) and followed by sequential dialysis against lysis buffers (without imidazole) containing 4 M, 2 M, and 1 M urea of pH 8.0. The protein was further dialyzed against distilled water to remove any remaining salts and subjected to lyophilization. Each step of the expression and purification process was followed by sodium dodecyl sulfate-polyacrylamide gel electrophoresis (SDS-PAGE) with visualization using Coomassie Brilliant Blue R-250. Densitometry was performed in ImageJ 1.53a [36] (National Institutes of Health, USA) to quantify protein purity.

2.2. Spinning dope preparation

Lyophilized Py_2W_2 protein powder was dissolved in a solution containing trifluoroacetic acid (TFA):2,2,2-trifluoroethanol (TFE):water (8:1:1 v:v:v) [9], with a final protein concentration of 25 % w:v. The resulting suspension was incubated for 30 min at room temperature with intermittent vortexing every 5 min for 5 s followed by centrifugation (20,817 rcf, 30 min, 10 °C) and the supernatant containing the solubilized Py_2W_2 was retained and used as a spinning dope. The supernatant was retained and used specifically to ensure that any residual particulate or precipitate that remains following the incubation and vortexing steps are not used for wet-spinning to prevent clogging of the extrusion needle.

2.3. Circular dichroism (CD) spectroscopy

In order to examine the solution-state secondary structure of the recombinant Py_2W_2 protein, building on protocols in prior studies on both Py_2 [3] and W_2 [5], far-ultraviolet (UV) CD spectra were collected in triplicate using a DSM20 CD spectrophotometer (Olis, Athens, GA, USA) at room temperature (22 °C ± 1 °C). 1 % (w:v) Py_2W_2 (~116 μM) was prepared in TFA:TFE:water (8:1:1 v:v:v) and CD spectra were acquired from 260 to 180 nm using integration time as a function of photomultiplier voltage with a 1 nm step size using quartz cuvette of 0.01 mm path length (Hellma Canada, Markham, ON, Canada) with all optical slits set at a bandpass of 5.0 nm. Blank subtraction was performed and the data were offset such that the average of ellipticity between over 250–260 nm was 0, with mean residue ellipticity ([θ]) [30] calculated and data reported as the average of triplicate measurement. Protein concentration was determined using absorbance at 214 nm and the molar extinction coefficient was estimated on the basis of the protein sequence (Fig. S1) using the Prot pi website server (https://www.protpi.ch/Calculator).

2.4. Wet-spinning of fibers

Fibers were spun using a home-built [3] automated wet-spinning apparatus at 28 ± 2 °C and 27 ± 3 % relative humidity, following previously established methods [3,4,29]. The dope solution containing 25 % w:v Py_2W_2 was loaded into a syringe (Hamilton Company, Reno, NV, USA) with 0.127 mm inner needle diameter and extruded into a coagulation bath containing 95 % ethanol (EtOH) at an extrusion rate of 600 μL/h. Fibers formed in the coagulation bath were picked up using tweezers and manually guided onto a roller with rotation speed matched to the extrusion rate so as not to stretch the resulting fiber. Fibers were either collected immediately in the "as-spun" (AS) state or subjected to various post-spin stretching conditions. For post-spin stretching, additional roller(s) were used with rotation speeds of either 2 × or 4 × as compared to the extrusion rate-matched roller. Fibers from six distinct post-spin stretching conditions were collected: a 2 × or 4 × stretch in air (2 × - or 4 × -air), a 2 × or 4 × stretch after submersion in water (2 × or 4 × -water), or a 2 × or 4 × stretch after submersion in 40 % EtOH (2 × - or 4 × -EtOH). SDS-PAGE was used to compare the protein dope solution before and after spinning fibers to test the protein integrity upon incubation in the acidic dope solvent.

2.5. Fiber imaging

After the spinning process, fibers were allowed to air-dry on the collection roller overnight at room temperature (~22 ± 1 °C). Fiber imaging was performed following protocols used in previous studies of pyriform [3] and aciniform [4,29] silks. Specifically, fibers of 1 cm length were secured onto U-shaped paper holders attached to a glass slide by tape. Optical imaging was performed (Axio Observer A1; Carl Zeiss Canada Ltd.; North York, ON, Canada) at 100 × magnification with 3 micrographs acquired per fiber, one near the middle and two near each end of the fiber. Fiber diameters were measured at six different positions per micrograph using ImageJ with the diameter based upon the average of the 18 measurements. Fibers were examined by polarized light microscopy using Axio Observer A1 equipped with a rotatable stage, a fixed analyzer slider, and a 90° rotatable polarizer D (Carl Zeiss Canada Ltd.). Fibers were oriented at ~45° with respect to plane polarized incident light prior to image capture.

Samples for scanning electron microscopy (SEM) were prepared following previous protocols [3,4], with fibers secured on an SEM stub using a conductive adhesive tape. All fibers were sputter-coated (EM ACE200; Leica Microsystems Inc.; Richmond Hill, ON, Canada) with a 5 nm thick layer of Au/Pd particles and images were collected up to 3000 × magnification (LEO1455VP SEM, Carl Zeiss Canada Ltd.). For transmission electron microscopy (TEM) samples, fibers were first fixed with 2.5 % glutaraldehyde diluted with 0.1 M sodium cacodylate buffer for at least 2 h, followed by rinsing three times for 10 min with 0.1 M sodium cacodylate buffer. Fibers were then fixed with 1 % osmium tetroxide, immediately followed by rinsing with distilled water, and then incubated in 0.25 % uranyl acetate at 4 °C overnight. Fibers were dehydrated with a graduated series of acetone, infiltrated with Epon araldite resin, and cured at 60 °C for 48 h. Thin sections of fibers were cut using an Ultracut E Ultramicrotome (Reichert-Jung, Heidelberg, Germany) with a diamond knife and placed on copper grids. Staining was performed with 2 % aqueous uranyl acetate (10 min), followed by rinsing (distilled water, 5 min, repeated twice), exposure to 0.3 % aqueous lead citrate (4 min), a quick rinse with distilled water, and air drying. Fibers were viewed using a JEM-1230 TEM (JEOL, Peabody, MA, USA) at 80 kV and images were captured using an Orca-HR digital camera (Hamamatsu, Bridgewater, NJ).

2.6. Mechanical testing

Mechanical testing was performed at 23 ± 2 °C and 45 ± 5 % relative humidity using a home-built apparatus, as described previously [3,4,29]. Fibers that had uniform diameter and surface morphology on the basis of optical microscopy were subjected to mechanical testing. The U-shaped paper frame was cut to free both ends of the fiber, with each end then clamped. One clamp was attached to a weight that was placed on an analytical balance (Mettler Toledo X5105DU, Greifensee, Switzerland) and the other clamp to a syringe pump (KD Scientific, model 100 series, Holliston, MA, USA) allowing for constant pulling of each fiber at a strain rate of 0.1 mm s^{-1}. The analytical balance allowed monitoring of weight change as a function of syringe pump displacement, allowing the determination of the applied force. The data were recorded using instrument-specific software (LabX, Mettler Toledo) and then exported to Excel 2023 (Microsoft, Seattle, WA) for further analysis. Engineering stress and strain were determined, alongside toughness and Young's modulus. Statistical significance of differences in mechanical parameters between the fibers from different conditions was evaluated using a two-tailed *t*-test with unequal variance in Excel 2023.

2.7. Fourier-transform infrared (FTIR) spectromicroscopy

Fibers collected from all conditions were mounted on glass slides. Spectra were collected using a Nicolet iN10 FTIR microscope (Thermo Fisher Scientific, Mississauga, ON, Canada) in attenuated total reflectance (ATR) mode at 4 cm^{-1} resolution over a spectral range of 400–4000 cm^{-1} with a total of 128 scans using a liquid nitrogen cooled detector [9]. For each condition, spectra were collected at two different regions for three different fibers, providing six distinct measurements for each condition. Spectra from each condition were baseline corrected, averaged, and processed using Origin (Learning Edition, OriginLab, Northampton, MA). The second derivative of the averaged spectrum of the amide I and amide II regions (considering ≈1475–1725 cm^{-1}) was calculated using a 13-point Savitzky–Golay algorithm and correlated with the absorbance spectrum over the same wavelength range to identify amide I and amide II bands related to protein secondary structure [9]. The same smoothing function and peak finding setting was applied in the amide I region with the Peak Deconvolution function in OriginPro to quantify the secondary structure content in the fibers, applying Gaussian line shapes and a threshold χ^2 of $<10^{-6}$ for convergence.

3. Results and discussion

3.1. Recombinant protein production and dope preparation

E. coli BL21(DE3) cells consistently produced high levels of Py_2W_2 after overnight expression at 20 °C, as observed by SDS-PAGE analysis (Fig. 2). Upon overexpression, Py_2W_2 was not soluble, likely accumulating in inclusion bodies (i.e., the lysis pellet lane in SDS-PAGE, Fig. 2) and was thus purified under denaturing conditions using Ni^{+2} affinity chromatography. The purification process resulted in a relatively pure protein (estimated purity of >90 %, assessed by ImageJ; Fig. 2). Expression was performed in M9 medium supplemented with amino acids, with the specific amino acids being selected based on their prevalence in the Py_2W_2 primary structure. Addition of amino acids to the culture medium led to a substantial increase in the yield of purified protein, with ~233 mg/L of culture vs. ~65 mg/L in LB medium. The approach of supplementing amino acids for enhancing recombinant protein production in *E. coli* has been reported in previous studies [37,38]. This reduces metabolic burden on the cells [39], leading to an

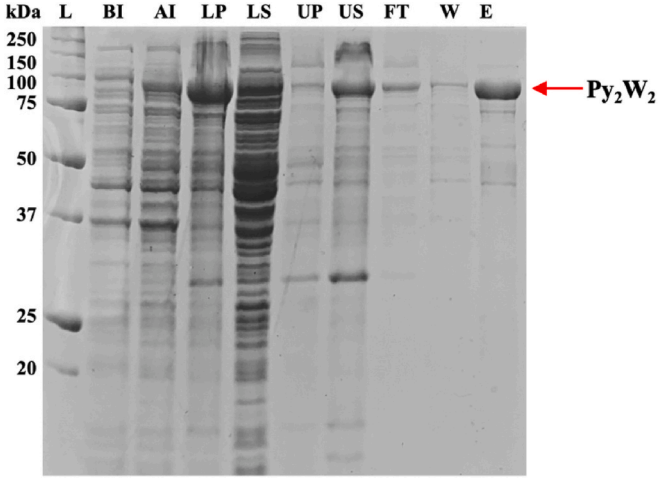

Fig. 2. Coomassie blue stained SDS-PAGE gel following the over-expression and purification of Py_2W_2 (target protein indicated with red arrow). The purified yield of Py_2W_2 is ~233 mg/L of *E. coli* culture using M9 medium with amino acid supplementation. Lane markers: molecular weight ladder with component molecular weights indicated in kDa (L); total cellular protein before (BI) and after (AI) induction; pellet (LP) and supernatant (LS) following cell lysis; pellet (UP) and supernatant (US) following resuspension of insoluble lysis fraction in denaturing urea buffer (i.e., following resuspension of LP); and, Ni^{2+}-affinity chromatography flow-through (FT), wash (W) and elution (E). (For interpretation of the references to color in this figure legend, the reader is referred to the Web version of this article.)

increase in cell mass and, consequently, an increase in the yield of recombinant protein. A recent study also demonstrated increased recombinant MA silk expression yields in *Bacillus megaterium* through targeted amino acid supplementation in minimal medium [40], implying that this is a more generally useful strategy for different expression hosts and silks. Notably, the molecular weight of Py_2W_2 is ~86.4 kDa meaning that this approach proved successful in increasing the yield of a relatively large-sized recombinant silk protein.

Previously, wet-spinning of recombinant pyriform and aciniform silk was performed in spinning dopes of TFA:TFE:water at a ratio of 3:1:1 (v:v:v) [3,29]. Increasing the concentration of TFA in the dope solution (TFA:TFE:water at 8:1:1, v:v:v), a composition found to enhance homogeneous film formation by a functionalized aciniform-MA fusion protein [9], allowed solubilization of Py_2W_2 at high concentration (25 % w/v). Films of aciniform-MA silk fusion protein that were deposited from this solvent combination also enabled viable PC12 cell growth and neuritogenesis [9], implying the potential broader suitability of this spinning dope for downstream biological application. Further supporting the utility of this spinning dope composition, the protein was found to be stable in these conditions, as observed by SDS-PAGE analysis (Fig. S2). The enhanced ability to solubilize Py_2W_2 through use of a higher relative TFA proportion is likely coming from the ability of TFA to act as both a hydrogen bond donor and acceptor and its propensity to break intra- and inter-molecular H-bonds, with potential to promote oligomer to monomer formation to solubilize otherwise recalcitrant species such as amyloidogenic Aβ(1–42) [41,42]. A higher TFA proportion thus likely increases Py_2W_2 solubility through a propensity to disrupt intermolecular β-sheet formation and dissociate oligomeric species that may remain following lyophilization, with the added benefit that it is a relatively volatile solvent [41,43].

Lyophilized Py_2W_2 dissolved in this dope solution was analyzed using far-UV CD spectroscopy. The observed positive band at 190 nm and negative bands at 208 nm and 222 nm (Fig. 3) indicate that Py_2W_2 has substantial α-helical content in the dope solution [44]. This is consistent with the previously reported secondary structure of W_2 [5], W_3 [29] and Py_2 [3] in buffer and spinning dope solutions.

3.2. Fiber wet-spinning and morphological characterization

Wet-spinning was achieved using the above-noted dope solution consisting of 25 % w:v Py_2W_2 dissolved in TFA:TFE:H_2O (8:1:1 v:v:v) and extruded into a 95 % EtOH coagulation bath. This spinning configuration proved to be amenable to continuous fiber formation. Fibers were collected either in the AS state or following subjection to six distinct post-spin stretching conditions. Fibers were imaged by optical microscopy (representative micrographs in Fig. 4), and any fibers with anomalies were rejected for downstream analysis during this step. Each

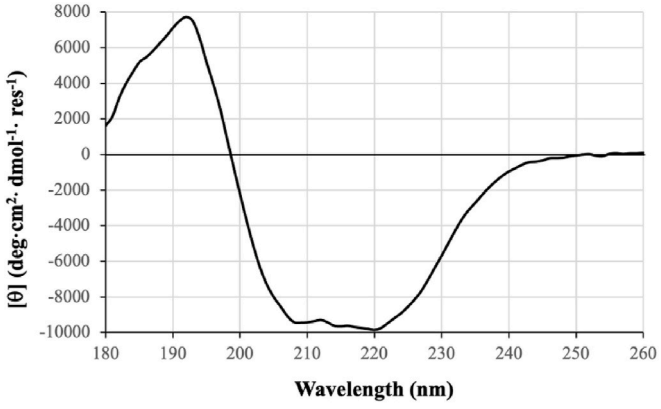

Fig. 3. Far-UV CD spectrum of Py_2W_2 in dope solution (~116 μM or 1 % w/v protein in TFA:TFE:H_2O; 8:1:1 v:v:v).

spinning condition led to fibers of generally uniform diameters, with AS fibers having the largest diameter (26.7 ± 1.40 μm) and with a decrease in diameter consistently observed upon post-spin stretching, with smaller diameters as the draw ratio was increased from 2 × to 4 × (Table 1).

Polarized light microscopy was used to assess the degree of molecular orientation and alignment relative to the fiber axis in each type of fiber (Fig. 4). A notable difference in anisotropy was observed between AS and post-spin stretched fibers, with AS fibers exhibiting a lower degree of anisotropy indicative of lower overall molecular orientation within the fibers and consistent with other silks (e.g., Refs. [3,4,29,45,46]). In comparison to AS fibers, the degree of anisotropy increased with post spin-stretching conditions, demonstrating condition-dependent differences. Stretching in air led to the smallest increase in anisotropy relative to the AS state, while the anisotropy induced by submersion in water prior to stretching was intermediate, and that following submersion in 40 % ethanol was greatest. This is consistent with increased molecular orientation for all post-spin stretching conditions, with the greatest overall degree of molecular orientation in ethanol-treated fibers.

A hallmark feature of post-spin stretching is an increase in anisotropy and structural orientation within silk fibers, whether in air [47] or solvent [4,29,46]. Improved fiber homogeneity (i.e., stretching-induced loss of defects) has been proposed to be key in this process [47], consistent with exclusion of spinning dope solvent retained in as-spun fibers but excluded during post-spin stretching with W_3 [4]. The increased anisotropy observed through post-spin stretching in solvent vs. in air seen here (Fig. 4) is consistent with the observation that exposure to an appropriate solvent during post-spin stretching specifically increases orientation of secondary structural units (e.g., β-sheets and, potentially, α-helices) in various recombinant silk fibers [4,29,46]. Notably, this was observed even in instances where the stretching process did not change the proportions of secondary structure types [46]. It is therefore possible that solvent exposure during post-spin stretching serves to increase intra-fiber dynamics, perhaps by transiently plasticizing the material (consistent with mechanisms proposed by Stengel et al. in hydration-induced β-sheet formation in aciniform silk [48]), enabling better rearrangement of secondary structural units than is achieved through stretching in air.

The surface morphology of each fiber type was examined by SEM, demonstrating cross-sections that are typically somewhat irregular in shape (i.e., not circular) regardless of spinning condition. This is consistent with wet-spun fibrillar morphologies observed for both Py_2 [3] and W_3 [4,29], noting that Py_2 fibers tend to be more irregular and heterogeneous than either W_3 or Py_2W_2 fibers. This likely arises from a hierarchical assembly process with stable fibrillar subunits that comprise the mature fiber, consistent also with observation by SEM of striations, ridges, and grooves parallel to the fiber long-axis in all instances (Fig. 4). AS fibers and those stretched in air also exhibited a rough surface, with the presence of nanostructures evident on the fiber surfaces (Fig. 4). These rough surface features were less apparent in water-treated fibers, while ethanol-treated fibers displayed smoother surfaces still, suggesting that fibrillar supramolecular assembly state depends on post-spin stretching conditions.

Using TEM, cross-sectional sections of 4 × -EtOH fibers were analyzed. This demonstrated a homogeneous electron density in the fibers (Fig. S3), indicative of a uniform distribution of molecules and of tight packing and defect-free fibers being achieved post-spin stretching. In contrast, previous TEM analysis of natural MA silk from *Nephila madagascariensis* demonstrated a core-skin structuring, characterized by a thin outer skin layer with higher electron density surrounding a homogeneous core of material with lower electron density [49]. The heterogeneous structure in this natural silk was attributed to fiber components produced in two discrete silk secreting regions of *Nephila* silk glands [49]. The recombinant Py_2W_2 silk thus lacks the skin-core structure observed in natural silk, consistent both with its being

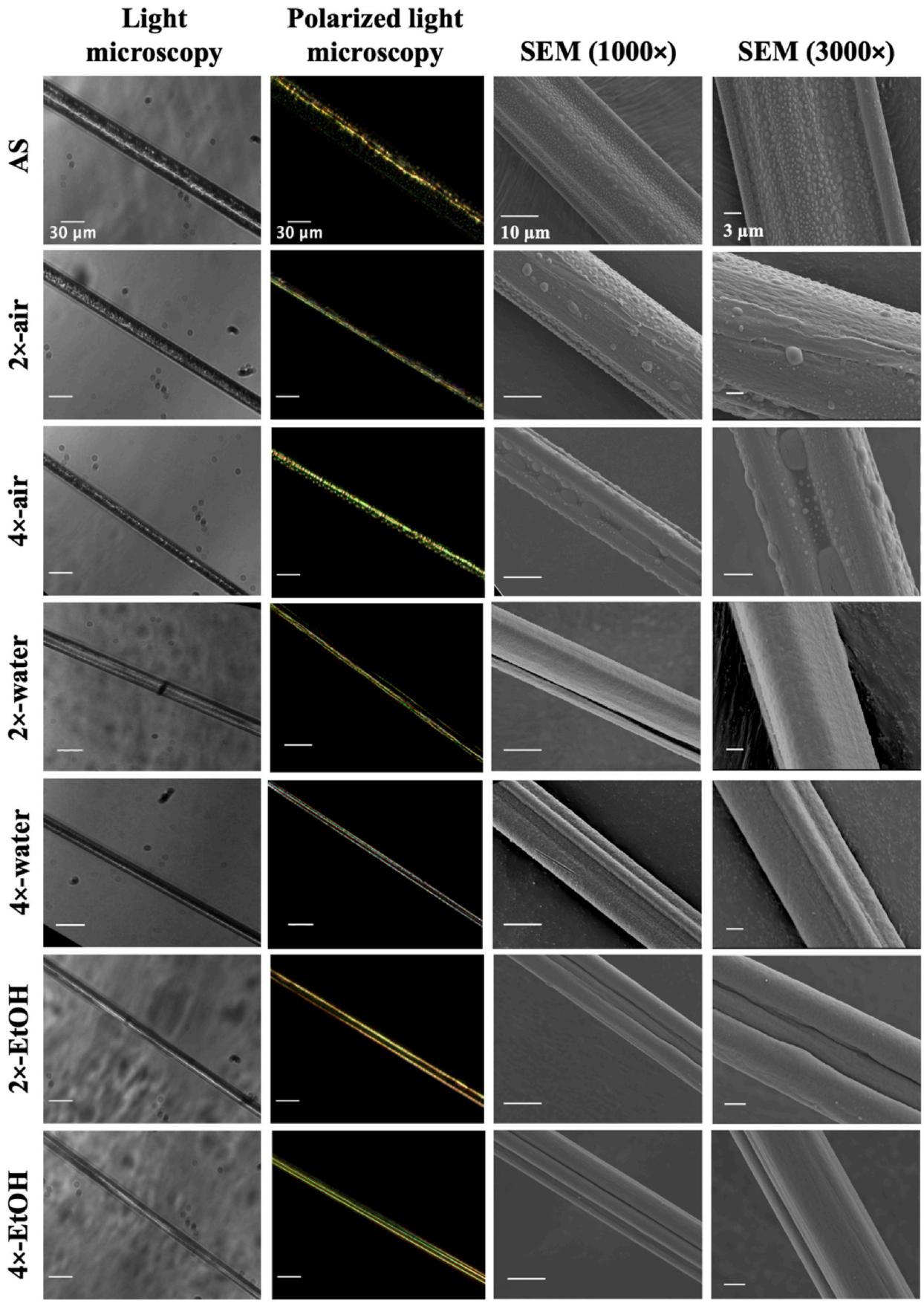

Fig. 4. Representative micrographs for indicated technique of wet-spun Py_2W_2 fibers (as-spun (AS) or post-spun stretched in automated manner at noted draw ratio in air or following immersion in water or 40 % ethanol (EtOH)). Scale bar dimensions are consistent per column.

Table 1
Mechanical properties and diameters of Py_2W_2 fibers spun under indicated conditions, noting that ultimate tensile strength is reported. Average and standard deviation are reported for n fibers of a given type.

Fiber type	Strength (MPa)	Extensibility (%)	Toughness ($MJ \cdot m^{-3}$)	Modulus (GPa)	Diameter (μm)	n
AS	28.3 ± 5.0	5.8 ± 2.2	1.1 ± 0.6	0.9 ± 0.1	26.7 ± 1.4	10
2×-air	48.3 ± 8.2	156.8 ± 38.3	58.3 ± 15.8	1.2 ± 0.2	17.8 ± 1.5	13
2×-water	55.7 ± 14.2	138.6 ± 35.8	65.0 ± 21.3	1.5 ± 0.4	20.5 ± 1.9	10
2×-EtOH	70.1 ± 14.6	93.2 ± 33.1	56.0 ± 22.7	1.8 ± 0.3	15.8 ± 1.1	8
4×-air	69.0 ± 8.5	27.9 ± 8.0	16.0 ± 4.8	2.0 ± 0.3	13.8 ± 1.0	18
4×-water	89.5 ± 14.5	74.5 ± 20.8	56.3 ± 18.6	1.8 ± 0.3	15.5 ± 1.4	10
4×-EtOH	130.7 ± 16.1	37.9 ± 17.3	41.0 ± 22.1	2.3 ± 0.4	14.3 ± 1.0	12

composed of a single type of spidroin and also with uniform molecular and fibrillar packing and architecture throughout fibers subjected to 4 × -EtOH post-spin stretching.

3.3. Mechanical characterization of fibers

A comprehensive comparison of the mechanical properties of Py_2W_2 fibers was conducted through tensile testing (Fig. 5, S4, and Table 1). Similar to other wet-spun recombinant silk fibers [3,19,29,50], the AS fibers exhibited the lowest strength (28.3 ± 5.0 MPa) and extensibility (5.8 ± 2.2 %). Regardless of the conditions employed, post-spin stretching significantly improved the mechanical properties of the fibers (statistical comparisons shown in Tables S2–S5). Among all the post-spin stretched fibers, the highest tensile strength and stiffness (i.e., Young's modulus) were observed for 4 × -EtOH fibers, at 130.7 ± 16.1 MPa (~4-fold stronger than AS fibers) and 2.3 ± 0.4 GPa (~2.5-fold higher than AS fibers), respectively. The 2 × -air fiber processing condition led to the highest extensibility, with 156.8 ± 38.3 % (~30-fold more extensible than AS fibers), and – correspondingly – the highest toughness, at 58.3 ± 15.8 MJ m^{-3} (~30 fold-tougher than AS fibers). Water-treated fibers exhibited mechanical properties falling between those of air-stretched and ethanol-treated fibers.

As a whole, Py_2W_2 fibers exhibited consistent trends in mechanical properties as a function of spinning conditions (Fig. 5, Table 1). First,

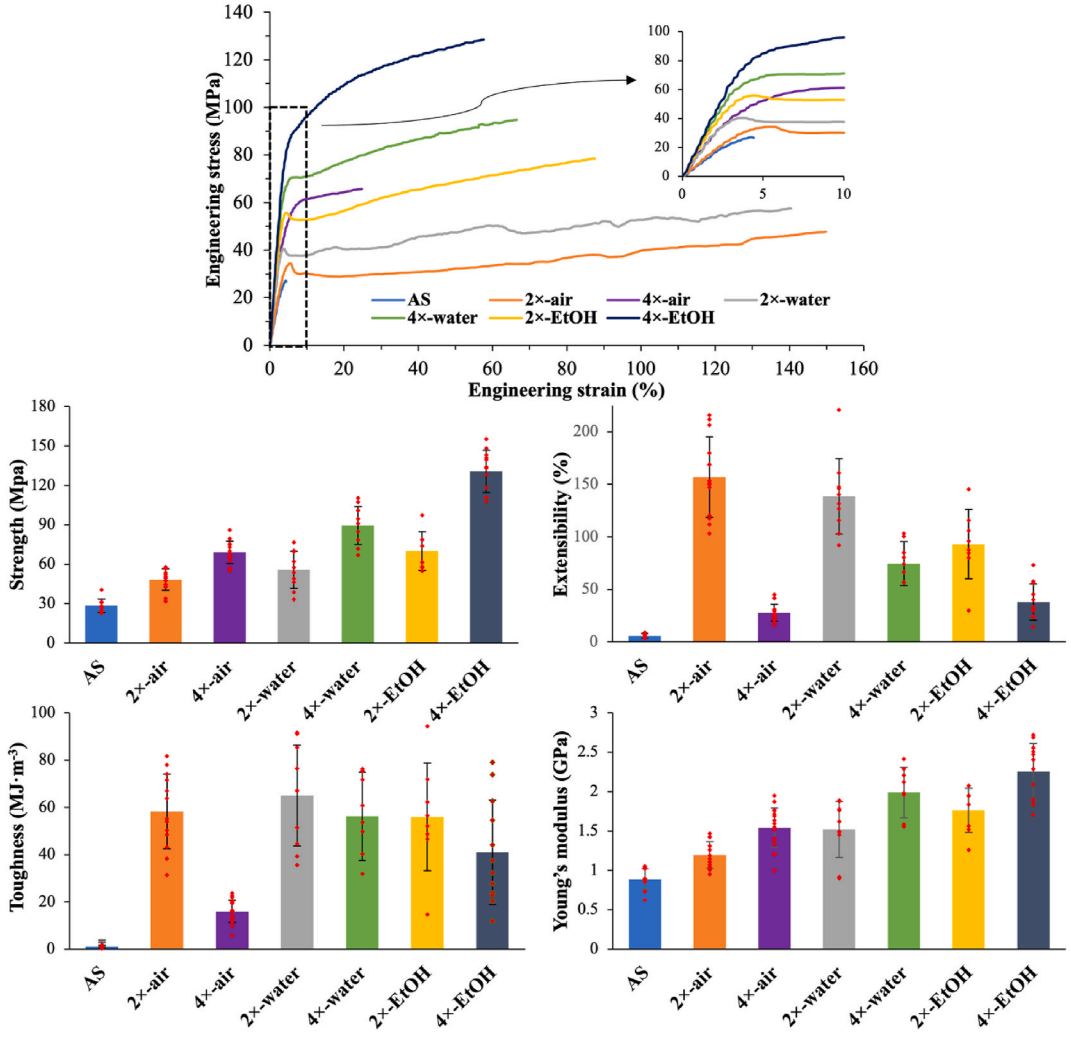

Fig. 5. Representative stress-strain curves (with inset plot showing region indicated by dashed box) and measured mechanical properties of Py_2W_2 fibers spun under indicated conditions. Individual data points (red dots) are included in the bar graphs, with bars being the mean and error bars the standard deviation. (For interpretation of the references to color in this figure legend, the reader is referred to the Web version of this article.)

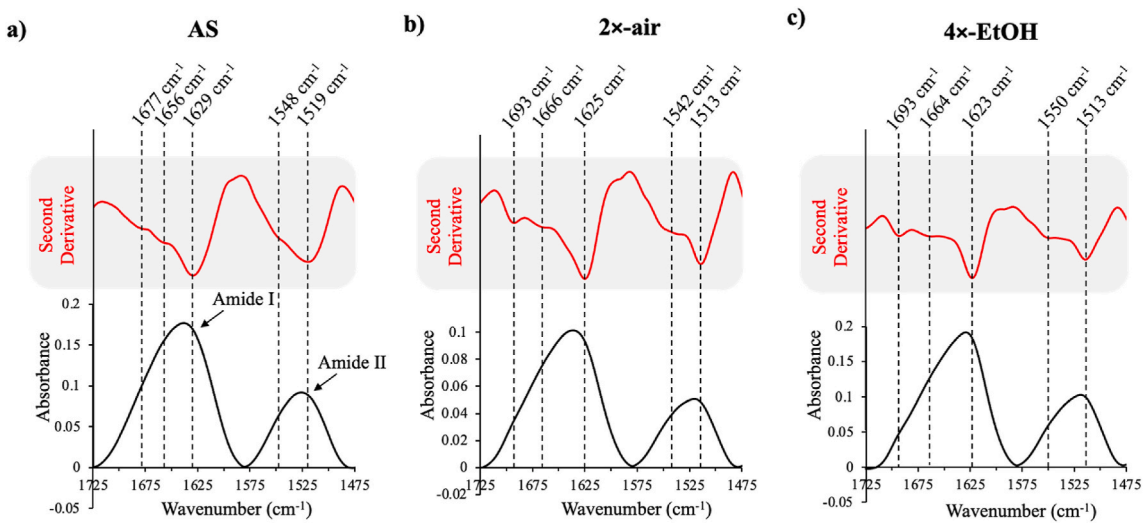

Fig. 6. Attenuated total reflectance-Fourier transform infrared spectromicroscopy of Py_2W_2 fibers spun under indicated conditions, showing amide I (~1600-1700 cm^{-1}) and amide II (~1500-1600 cm^{-1}) band regions (full spectra are shown in Fig. S5). Second derivatives were calculated and smoothed using a 13-point Savitzky–Golay algorithm. The primary amide I and amide II components observed in the second derivative are annotated and shown with dashed lines, with each reported spectrum being the average of six measured spectra (two acquired with the ATR probe positioned at different locations on each of three fibers from each condition).

regardless of the solvent used, an increase in draw ratio led to a significant (Table S2) increase in strength. Conversely, as the draw ratio was increased, extensibility significantly (Table S3) decreased, with the largest decrease factor seen for air stretched fibers and the smallest for water-stretched fibers. This behavior is consistent with the effects of post-spin draw ratio seen with other silks drawn in air [47] or solvent [45]. The Young's modulus was also observed to increase from the AS state to post-spin stretched states, with an increase in draw ratio uniformly leading to increased stiffness (Table 1) but with differences observed between draw ratios for a given post-spin stretching solvent not always being significant (Table S5). Finally, although toughness was significantly increased from AS to any of the post-spun stretched conditions, this is not as straightforwardly related to draw ratio as it couples contributions from both strength and extensibility.

The mechanical behavior observed as a function of fiber processing correlated well with the degree of anisotropy observable by polarized light microscopy. The subpar mechanical properties of the AS fibers are consistent with a relatively poorly organized molecular orientation, resulting in the observed low anisotropy. Conversely, the highest degree of polarization consistent with a high degree of molecular anisotropy was observed in the 4 × -EtOH fibers which, were the strongest fibers. In all, both exposure of fibers to solvents, such as water or ethanol, followed by stretching clearly induced molecular-level rearrangement in the fibers.

3.4. Fiber-state secondary structure determination

Py_2W_2 fiber-state secondary structure was evaluated using ATR-FTIR spectromicroscopy, second derivative analysis, and amide I peak deconvolution. Second derivative analysis was used for identification of overlapped bands in the amide I and amide II regions, whereas deconvolution of the amide I region was used to calculate the content of secondary structures present in each fiber type. Based on the FTIR absorption and second derivative spectra (Fig. S5), distinct differences in the spectral patterns were observed as a function of fiber type. The most noteworthy variations were observed between AS and 4 × -EtOH fibers (Fig. 6). In the amide I region of AS fibers, a distinct peak minimum observed at 1629 cm^{-1} in the second derivative spectrum is characteristic of β-sheet content [51–53] and the weaker bands at 1656 cm^{-1}, and 1677 cm^{-1} are indicative of random coil/α-helix [51–54] and β-turn [52] components, respectively. In the case of 4 × -EtOH fibers, an intense peak at 1623 cm^{-1} attributable to β-sheets [51–54] and weak peaks at 1664 cm^{-1} and 1693 cm^{-1} were observed, attributable to β-turns [52]. The most extensible condition, 2 × -air, is shown for comparison (Fig. 6b). In this case, a similar structural transformation away from the AS state is observed to that in 4 × -EtOH, with the β-sheet peak at ~1623 cm^{-1} (4 × -EtOH) or ~1625 cm^{-1} being sharper for the stronger 4 × -EtOH condition than for the 2 × -air condition, consistent with the observed increase in strength.

Amide I band deconvolution (Table 2, Fig. S6) is consistent with the peak components identified by second derivative analysis (Fig. 6),

Table 2
Secondary structure content for indicated Py_2W_2 fiber type based upon attenuated total reflectance Fourier transform infrared spectromicroscopy amide I peak deconvolution.

Fiber type	Peak position (cm^{-1})	% amide I peak	Assignment [Citation(s)]
AS	1609	6	aggregated strands [52]
	1628	35	β-sheets [51–53]
	1657	51	random coils/α-helices [51–54]
	1689	8	β-turns [52]
2 × -air	1625	43	β-sheets [51–53]
	1658	50	random coils/α-helices [52,54]
	1691	7	β-turns [52]
4 × -EtOH	1625	52	β-sheet [51–53]
	1659	42	random coils/α-helices [51–54]
	1690	6	β-turns [52]

allowing quantitation of secondary structure. Both AS and 2 × -air fibers have a large contribution from random coil/α-helical structuring, and similar β-strand/sheet content with the distinction that an aggregated strand component is apparent in AS fibers which is lost upon stretching in air, likely implying better β-sheet alignment (43%). 4 × -EtOH fibers, conversely, exhibit the greatest β-sheet content and least random coil/α-helical content. Fibers from all three conditions have similar (6–8%) β-turn composition. Although deconvolution was not performed for all fiber types, similar spectral patterns with a strong peak component around 1625 cm^{-1} were observed in all conditions (Fig. S5), supporting the dominance of β-sheets as the major structural component.

While analysis of amide II FTIR peaks in silk has only been reported in a limited set of previous studies (e.g., Refs. [55,56]), distinctive spectral changes were evident between AS and 4 × -EtOH fibers. Second derivative minima at 1519 cm^{-1} (AS) and 1513 cm^{-1} (2 × -air and 4 × -EtOH) fibers indicated the presence of β-sheets [55]. The more intense and less broad peak at 1513 cm^{-1} in both of the post-spun stretched fibers suggested a higher β-sheet content as compared to AS fibers. Peaks around 1550 cm^{-1} in both the AS and 4 × -EtOH fibers are consistent with a convolution of an amorphous matrix composed of α-helices and random coils and β-sheet [55], while the shift of this peak to 1542 cm^{-1} in 2 × -air would be indicative of a greater amorphous contribution [55] which is consistent with the high degree of extensibility observed for this condition.

The second derivative analysis of both amide I and amide II regions and the deconvolution of amide I region provide clear evidence of a structural transition during the post-spin stretching treatment. This transition involves a depletion of random coil/α-helical content and an increase in β-sheet content. This contrasts with the behavior reported for recombinant dragline silk, where post-spin stretching did not enhance the proportion of β-sheet, strictly improving alignment and orientation of the β-sheet components [46]. The solvent-induced increase in β-sheet content observed for Py_2W_2 may in part arise from a plasticizing effect of solvent [46], as discussed above. EtOH has also specifically been proposed to promote β-sheet formation during silkworm silk post-spin stretching though dehydration of random coil segments of the protein leading to an enhanced propensity for intra- and intermolecular H-bonding interactions [57]. When coupled with the extensional forces resulting from the post-spin draw, this would in turn be likely to favor aligned β-sheet formation. In all, the secondary structure content of Py_2W_2 fibers correlate well with their mechanical properties. Namely, the 4 × -EtOH fibers, which exhibited the highest strength, also have highest β-sheet content, while the highly extensible 2 × -air fibers maintain amorphous content but exhibit better β-sheet ordering than the less strong AS fiber state.

3.5. Comparison of Py_2W_2 fibers with other recombinant and natural spider silks

When comparing structural features and mechanical properties of recombinant spider silks, it is important to note that these properties depend on a variety of factors. This includes the molecular weight of the constituent spidroins, concentration of spidroin in the spinning dope, composition of dope solution, spinning method, degree of post-spin stretching, and solvent treatment(s) [19,29]. Py_2W_2 fibers demonstrated distinct morphology and impressive strength and extensibility when compared to a diverse range of fibers previously spun from different recombinant spidroins.

Both pyriform and aciniform silk from *Trichonephila clavipes* were observed by polarized Raman spectromicroscopy to transform from an α-helix rich state in their respective glands to mixed α-helical/β-sheet/disordered state fibers [31]. Solid-state NMR was also used to demonstrate relatively α-helix rich fibers in aciniform silk from *A. argentata* [58] that become further enriched in β-sheet upon water exposure [48]. Both the W unit and Py unit have been shown to be mixtures of α-helical and intrinsically disordered segments that are devoid of β-sheet content in solution [27,30], with both types of recombinant spidroin undergoing structural transitions upon wet-spinning to fibers that retain disordered content, are partially depleted in α-helical content, and which have substantial β-sheet content [3,4,29]. A similar structural transformation is observed for Py_2W_2, with an α-helix-rich soluble state that converts to a β-sheet enriched fiber state. This implies that the Py unit and W unit are not perturbing to each other in the context of protein organization, intermolecular interactions, and structural transformation during wet-spinning of the chimeric fusion protein, with the β-sheet elements required to imbue strength in these silk fibers being readily formed in the context of favourable structural elements to support outstanding extensibility.

Comparing mechanics directly, silk fibers formed from the individual spidroins comprising Py_2W_2, the 47.9 kDa Py_2 (wet-spun [3]) and 38.0 kDa W_2 (hand-drawn [27]) proteins, exhibit strengths of up to 72.0 ± 5.0 MPa and 67.0 ± 16.0 MPa, respectively, along with extensibility of up to 27.6 ± 6.1 % and 31.0 ± 11.0 %, respectively. Allowing more straightforward comparison of spinning conditions, the larger W_3 protein has been wet-spun, with the best spinning conditions noted to date providing a strength of 100 ± 24 MPa and extensibility of 41 ± 13 [29]. The superior strength of Py_2W_2 fibers (i.e., up to ~82 % higher) compared to fibers formed by the constituent spidroins is consistent with the larger molecular weight of the monomeric spidroin in the fibers, although this is not a straightforwardly predictable outcome given the distinct protein composition and architecture for Py_2W_2 relative to either Py_2 or W_2 (Fig. 1). Notably, the up to 5-fold increase in extensibility observed for Py_2W_2 relative to either Py_2 or W_2 would also not be anticipated strictly on the basis of increased molecular weight. In W-unit based proteins, for example, extensibility does not scale with molecular weight, instead being relatively similar for W_4 and W_2 [28]. Natural aciniform silk from *A. trifasciata*, which would be W_{14} or larger flanked by non-repetitive N- and C-terminal domains, is much stronger (687 ± 56 MPa) but is less extensible (86 ± 3 %) [24] than Py_2W_2. Pyriform silk from *A. argentata* has not been characterized; to date, the only isolated natural pyriform fibers characterized are glue coated fibers from the ground spider *Drassodex heeri*, with strength of 511.0 ± 123.6 MPa and extensibility of 51 ± 26 % [59]. For comparison, Flag is known as the most extensible spider silk, with extensibility as high as ~476 % reported [60]. Compellingly, many natural Flag silks have similar or even lower extensibilities to that observed for 2 × -air Py_2W_2 fibers [61,62], indicating that this recombinant chimeric spidroin has clear promise in terms of being both an extensible and strong material.

From a morphological standpoint, Py_2W_2 fibers are intermediate in diameter (26.7 ± 1.4 μm, AS state) to wet-spun Py_2 (32.9 ± 4.5 μm) [3] and W_3 (23.0 ± 1.0 μm) [4] fibers. W_2, to date, has not been wet-spun, with hand-drawing of fibers from an aqueous buffer solution resulting in a considerably smaller diameter (1.5 ± 0.1 μm) [27]. Fiber cross-sectional profiles for the constituent proteins differ, with W_3 exhibiting a circular cross-section and Py_2 an irregular cross-section. Py_2W_2 fibers are most similar in shape and surface features to W_3 spun from a TFA/TFE/H_2O spinning dope. The observed decrease in surface roughness of Py_2W_2 fibers upon post-spin stretching is also similar to the observed changes for both Py_2 and W_3 fibers spun from TFA/TFE/H_2O-based dope solutions and post-spun stretched in 40 % ethanol (Py_2) or water (W_3).

Besides the noted variations in mechanical properties and fiber morphology, a significant distinction between the Py_2W_2 and Py_2 fibers is seen in water compatibility during the post-spin stretching treatment. Namely, Py_2W_2 fibers exhibited remarkable mechanical behavior with outstanding extensibility when stretched after submersion in water. In contrast, Py_2 fibers were unable to tolerate water during post-spin stretching [35], possibly arising from supercontraction as is observed in some other classes of spider silks [1]. The Py_2W_2 chimeric fusion protein therefore appears to maintain the excellent water compatibility of W-based proteins, despite being >50 % Py-based by mass.

Looking beyond the constituent proteins, Py_2W_2 fibers have

comparable strength and 4-fold higher extensibility compared to hand-drawn W_2Cma_2 (52.8 kDa) fibers [28], noting that these undergo a similar structural transformation and have a similar morphology. Chimeric silk fibers composed of $Flag_R$-$AcSp1_R$ (36.8 kDa), pulled from a buffered protein solution, had a relatively small diameter of 1.37 ± 0.18 μm, higher strength (261.4 ± 47.5 MPa) but lower extensibility (15.0 ± 8.0 %) when compared to Py_2W_2 fibers [33]. These fibers also exhibited a relatively low proportion of α-helical content (~11 %). Finally, wet-spun Flag-MA ($Y1S8_{20}$, 62 kDa) synthetic fibers exhibit strength ranges up to 123.0 ± 15.0 MPa and extensibility up to 57.3 ± 17.0 %, with these being tunable based on the post-spin processing conditions [32]. Py_2W_2 fibers thus show slightly superior strength and significantly greater extensibility as compared to $Y1S8_{20}$ fibers. Interestingly, $Y1S8_{20}$ fibers exhibited characteristics of both constituent spidroin types when water-treated, with no α-helical content being inferred by solid-state NMR. These are quite distinct, therefore, in terms of secondary structuring from other chimeric silks to date including Py_2W_2. The notable mechanical performance of Py_2W_2 fibers, which combines strength and extensibility, and which can be readily tuned through post-spin processing, positions them as a superior biomaterial compared to other individual or chimeric recombinant silk fibers.

3.6. Prospects for application

Depending upon spinning conditions, Py_2W_2 may be processed into fibers with both high strength and extensibility. With single filament diameters on the order of ~14–27 μm, it is likely that applications would be best enabled through braiding filaments together to form a thread or yarn. Given that spider silks are renowned for their biocompatibility and biodegradability, and that Py_2W_2 fibers are water compatible, threads composed of Py_2W_2 fibers may be particularly suited for application as surgical sutures following precedents with natural silks [13]. This would be enhanced through the straightforward ability to modulate the protein composition and to reproducibly produce consistent fibrillar materials through recombinant silk production in comparison to harvesting natural spider silks where one must rely on the native sequence and coax production of the fiber. It is also likely that 3D scaffolds could be formed from strong and tough Py_2W_2 fibers, with great potential in the field of regenerative medicine again following precedents for natural spider silk scaffolds [63]. The ability to modulate protein properties in this instance may be particularly beneficial, providing potential to specifically sequester target molecules that will enhance functionality [9]. Besides biomedical use, the mechanical behavior of Py_2W_2 fibers implies strong potential for application when woven into a net and used as impact-absorbing material [64]. In short, the capability to both dramatically tune mechanics for this recombinant silk (Fig. 5) and to readily enhance the protein composition should provide a versatile starting point for diverse applications.

4. Conclusion

In summary, this study provides the first investigation into silk fibers composed of chimeric proteins comprising repetitive modules from pyriform and aciniform silks, namely Py_2W_2. The expression of Py_2W_2 in culture medium supplemented with selected amino acids resulted in a high-level of protein production that was targeted to inclusion bodies and thus readily purified. Py_2W_2 was observed to have high α-helical content in a fluorinated acid/alcohol spinning dope solution, with the fiber formation process inducing a structural transition from α-helix to β-sheet, as evidenced by the FTIR spectromicroscopy. Post-spin stretching and solvent treatment further induced molecular rearrangement within the fibers, reflected by an increased degree of anisotropy and enhanced β-sheet content. The effects of post-spin stretching treatment were also manifest in the varied surface morphology and mechanical properties of the fibers. Py_2W_2 fibers exhibited a combination of high strength and high extensibility, which correlates well with the molecular anisotropy and the secondary structure contents within the fiber. The mechanical properties of Py_2W_2 fibers are superior compared to fibers spun from individual or other chimeric proteins, with the extensibility observed herein – and the resulting toughness – being particularly notable. Additionally, unlike Py_2 fibers, the fusion of Py_2 with W_2 rendered Py_2W_2 fibers water-compatible, suggesting an additional advantage of engineered chimeric spidroins over individual spidroins. These findings highlight the potential of hybrid silks for diverse applications, showcasing their versatility and adaptability in the realm of biomaterials.

CRediT authorship contribution statement

Anupama Ghimire: Writing – review & editing, Writing – original draft, Visualization, Methodology, Investigation, Funding acquisition, Formal analysis, Conceptualization. **Lingling Xu:** Writing – review & editing, Methodology, Investigation, Conceptualization. **Xiang-Qin Liu:** Writing – review & editing, Supervision, Funding acquisition, Conceptualization. **Jan K. Rainey:** Writing – review & editing, Writing – original draft, Visualization, Validation, Supervision, Methodology, Funding acquisition, Formal analysis, Conceptualization.

Declaration of competing interest

The authors declare the following financial interests/personal relationships which may be considered as potential competing interests: Jan K. Rainey reports a relationship with 3DBioFibR Inc. that includes: equity or stocks and funding grants. If there are other authors, they declare that they have no known competing financial interests or personal relationships that could have appeared to influence the work reported in this paper.

Data availability

Data will be made available on request.

Acknowledgments

We are grateful to Mary Ann Trevors (Electron Microscopy CORE Facility, Dalhousie University) for expert guidance, training and assistance with electron microscopy, Jack Wuotila (Department of Biochemistry & Molecular Biology, Dalhousie University) for valuable help during BIOC 3620 - Experiential Learning, and Sophie Haverstock (Department of Biochemistry & Molecular Biology, Dalhousie University) for technical assistance. AG particularly wants to thank all members of the Rainey lab for their kind support.

This work was supported by the Natural Sciences and Engineering Research Council of Canada (NSERC; grants RGPIN-2020-06083 to X-QL and RGPIN-2023-05912 to JKR) and the NSERC CREATE Training Program in BioActives (510963). Key infrastructure was provided by NSERC Research Tools and Instruments Grants and Dalhousie Medical Research Foundation Capital Equipment Grants. AG is the recipient of a Doctoral level Nova Scotia Graduate Scholarship.

Appendix A. Supplementary data

Supplementary data to this article can be found online at https://doi.org/10.1016/j.mtbio.2024.101073.

References

[1] S.J. Blamires, T.A. Blackledge, I.M. Tso, Physicochemical property variation in spider silk: ecology, evolution, and synthetic production, Annu. Rev. Entomol. 62 (2017) 443–460, https://doi.org/10.1146/annurev-ento-031616-035615.

[2] J.M. Gosline, P.A. Guerette, C.S. Ortlepp, K.N. Savage, The mechanical design of spider silks: from fibroin sequence to mechanical function, J. Exp. Biol. 202 (1999) 3295–3303, https://doi.org/10.1242/jeb.202.23.3295.

[3] J.R. Simmons, L. Xu, J.K. Rainey, Recombinant pyriform silk fiber mechanics are modulated by wet-spinning conditions, ACS Biomater. Sci. Eng. 5 (2019) 4985–4993, https://doi.org/10.1021/acsbiomaterials.9b00504.

[4] N. Weatherbee-Martin, L. Xu, A. Hupe, L. Kreplak, D.S. Fudge, X.-Q. Liu, J. K. Rainey, Identification of wet-spinning and post-spin stretching methods amenable to recombinant spider aciniform silk, Biomacromolecules 17 (2016) 2737–2746, https://doi.org/10.1021/acs.biomac.6b00857.

[5] L. Xu, J.K. Rainey, Q. Meng, X.-Q. Liu, Recombinant minimalist spider wrapping silk proteins capable of native-like fiber formation, PLoS One 7 (2012) e50227, https://doi.org/10.1371/journal.pone.0050227.

[6] F. Teulé, A.R. Cooper, W.A. Furin, D. Bittencourt, E.L. Rech, A. Brooks, R.V. Lewis, A protocol for the production of recombinant spider silk-like proteins for artificial fiber spinning, Nat. Protoc. 4 (2009) 341–355, https://doi.org/10.1038/nprot.2008.250.

[7] D. Hümmerich, U. Slotta, T. Scheibel, Processing and modification of films made from recombinant spider silk proteins, Appl Phys A 82 (2006) 219–222, https://doi.org/10.1007/s00339-005-3428-5.

[8] U. Slotta, M. Tammer, F. Kremer, P. Koelsch, T. Scheibel, Structural analysis of spider silk films, Supramol. Chem. 18 (2006) 465–471, https://doi.org/10.1080/10610270600832042.

[9] L.A. Baker, L. Xu, F. Badichi Akher, M.K. Robertson, L. Pugsley-DeBruyn, C.X. Ma, X.Q. Liu, J.P. Frampton, J.K. Rainey, Nerve growth factor-binding engineered silk films promote neuronal attachment and neurite outgrowth, Adv. Funct. Mater. 32 (2022) 2205178, https://doi.org/10.1002/adfm.202205178.

[10] K. Schacht, T. Scheibel, Controlled hydrogel formation of a recombinant spider silk protein, Biomacromolecules 12 (2011) 2488–2495, https://doi.org/10.1021/bm200154k.

[11] A. Lammel, M. Schwab, M. Hofer, G. Winter, T. Scheibel, Recombinant spider silk particles as drug delivery vehicles, Biomaterials 32 (2011) 2233–2240, https://doi.org/10.1016/j.biomaterials.2010.11.060.

[12] M. Hofer, G. Winter, J. Myschik, Recombinant spider silk particles for controlled delivery of protein drugs, Biomaterials 33 (2012) 1554–1562, https://doi.org/10.1016/j.biomaterials.2011.10.053.

[13] K. Hennecke, J. Redeker, J.W. Kuhbier, S. Strauss, C. Allmeling, C. Kasper, K. Reimers, P.M. Vogt, Bundles of spider silk, braided into sutures, resist basic cyclic tests: potential use for flexor tendon repair, PLoS One 8 (2013) e61100, https://doi.org/10.1371/journal.pone.0061100.

[14] S. Salehi, K. Koeck, T. Scheibel, Spider silk for tissue engineering applications, Molecules 25 (2020) 737, https://doi.org/10.3390/molecules25030737.

[15] C. Holland, K. Numata, J. Rnjak-Kovacina, F.P. Seib, The biomedical use of silk: past, present, future, Adv. Healthcare Mater. 8 (2019) 1800465, https://doi.org/10.1002/adhm.201800465.

[16] F.G. Omenetto, D.L. Kaplan, New opportunities for an ancient material, Science 329 (2010) 528–531, https://doi.org/10.1126/science.1188936.

[17] C. Guo, C. Li, X. Mu, D.L. Kaplan, Engineering silk materials: from natural spinning to artificial processing, Appl. Phys. Rev. 7 (2020), https://doi.org/10.1063/1.5091442.

[18] W. He, D. Qian, Y. Wang, G. Zhang, Y. Cheng, X. Hu, K. Wen, M. Wang, Z. Liu, X. Zhou, M. Zhu, A protein-like nanogel for spinning hierarchically structured artificial spider silk, Adv Mater 34 (2022) e2201843, https://doi.org/10.1002/adma.202201843.

[19] B. Schmuck, G. Greco, F.G. Bäcklund, N.M. Pugno, J. Johansson, A. Rising, Impact of physio-chemical spinning conditions on the mechanical properties of biomimetic spider silk fibers, Commun Mater 3 (2022) 83, https://doi.org/10.1038/s43246-022-00307-6.

[20] K. Arakawa, N. Kono, A.D. Malay, A. Tateishi, N. Ifuku, H. Masunaga, R. Sato, K. Tsuchiya, R. Ohtoshi, D. Pedrazzoli, 1000 spider silkomes: linking sequences to silk physical properties, Sci. Adv. 8 (2022) eabo6043, https://doi.org/10.1126/sciadv.abo6043.

[21] J.L. Yarger, B.R. Cherry, A. Van Der Vaart, Uncovering the structure–function relationship in spider silk, Nat. Rev. Mater. 3 (2018) 1–11, https://doi.org/10.1038/natrevmats2018.8.

[22] L. Römer, T. Scheibel, The elaborate structure of spider silk: structure and function of a natural high performance fiber, Prion 2 (2008) 154–161, https://doi.org/10.4161/pri.2.4.7490.

[23] N.A. Ayoub, J.E. Garb, R.M. Tinghitella, M.A. Collin, C.Y. Hayashi, Blueprint for a high-performance biomaterial: full-length spider dragline silk genes, PLoS One 2 (2007) e514, https://doi.org/10.1371/journal.pone.0000514.

[24] C.Y. Hayashi, T.A. Blackledge, R.V. Lewis, Molecular and mechanical characterization of aciniform silk: uniformity of iterated sequence modules in a novel member of the spider silk fibroin gene family, Mol. Biol. Evol. 21 (2004) 1950–1959, https://doi.org/10.1093/molbev/msh204.

[25] E. Blasingame, T. Tuton-Blasingame, L. Larkin, A.M. Falick, L. Zhao, J. Fong, V. Vaidyanathan, A. Visperas, P. Geurts, X. Hu, Pyriform spidroin 1, a novel member of the silk gene family that anchors dragline silk fibers in attachment discs of the black widow spider, *Latrodectus hesperus*, J. Biol. Chem. 284 (2009) 29097–29108, https://doi.org/10.1074/jbc.M109.021378.

[26] R.C. Chaw, C.A. Saski, C.Y. Hayashi, Complete gene sequence of spider attachment silk protein (PySp1) reveals novel linker regions and extreme repeat homogenization, Insect Biochem. Mol. Biol. 81 (2017) 80–90, https://doi.org/10.1016/j.ibmb.2017.01.002.

[27] M.-L. Tremblay, L. Xu, T. Lefèvre, M. Sarker, K.E. Orrell, J. Leclerc, Q. Meng, M. Pézolet, M. Auger, X.-Q. Liu, Spider wrapping silk fibre architecture arising from its modular soluble protein precursor, Sci. Rep. 5 (2015) 11502, https://doi.org/10.1038/srep11502.

[28] L. Xu, T. Lefèvre, K.E. Orrell, Q. Meng, M. Auger, X.-Q. Liu, J.K. Rainey, Structural and mechanical roles for the C-terminal nonrepetitive domain become apparent in recombinant spider aciniform silk, Biomacromolecules 18 (2017) 3678–3686, https://doi.org/10.1021/acs.biomac.7b01057.

[29] L. Xu, N. Weatherbee-Martin, X.Q. Liu, J.K. Rainey, Recombinant silk fiber properties correlate to prefibrillar self-assembly, Small 15 (2019) 1805294, https://doi.org/10.1002/smll.201805294.

[30] J.R. Simmons, G. Gasmi-Seabrook, J.K. Rainey, Structural features, intrinsic disorder, and modularity of a pyriform spidroin 1 core repetitive domain, Biochem. Cell. Biol. 101 (2023) 271–283, https://doi.org/10.1139/bcb-2022-0338.

[31] T. Lefèvre, S. Boudreault, C. Cloutier, M. Pézolet, Diversity of molecular transformations involved in the formation of spider silks, J. Mol. Biol. 405 (2011) 238–253, https://doi.org/10.1016/j.jmb.2010.10.052.

[32] F. Teulé, B. Addison, A.R. Cooper, J. Ayon, R.W. Henning, C.J. Benmore, G. P. Holland, J.L. Yarger, R.V. Lewis, Combining flagelliform and dragline spider silk motifs to produce tunable synthetic biopolymer fibers, Biopolymers 97 (2012) 418–431, https://doi.org/10.1002/bip.21724.

[33] L.Y. Tian, Q. Meng, Y. Lin, Expression and characterization of chimeric spidroins from flagelliform-aciniform repetitive modules, Biopolymers 111 (2020) e23404, https://doi.org/10.1002/bip.23404.

[34] M.-L. Tremblay, L. Xu, M. Sarker, X.-Q. Liu, J.K. Rainey, Characterizing aciniform silk repetitive domain backbone dynamics and hydrodynamic modularity, Int. J. Mol. Sci. 17 (2016) 1305, https://doi.org/10.3390/ijms17081305.

[35] J.R. Simmons, From Soluble Protein to Anchoring Filament: Understanding the Structural and Mechanical Foundations of Pyriform Spider Silk, Dalhousie University, 2022. Doctoral Thesis.

[36] C.A. Schneider, W.S. Rasband, K.W. Eliceiri, NIH Image to ImageJ: 25 years of image analysis, Nat. Methods 9 (2012) 671–675, https://doi.org/10.1038/nmeth.2089.

[37] J. Kumar, A.S. Chauhan, R.L. Shah, J.A. Gupta, A.S. Rathore, Amino acid supplementation for enhancing recombinant protein production in *E. coli*, Biotechnol. Bioeng. 117 (2020) 2420–2433, https://doi.org/10.1002/bit.27371.

[38] D.C. Chow, M.R. Dreher, K. Trabbic-Carlson, A. Chilkoti, Ultra-high expression of a thermally responsive recombinant fusion protein in *E. coli*, Biotechnol. Prog. 22 (2006) 638–646, https://doi.org/10.1021/bp0503742.

[39] J. Heyland, L.M. Blank, A. Schmid, Quantification of metabolic limitations during recombinant protein production in *Escherichia coli*, J. Biotechnol. 155 (2011) 178–184, https://doi.org/10.1016/j.jbiotec.2011.06.016.

[40] A. Connor, R.H. Zha, M. Koffas, Production and secretion of recombinant spider silk in *Bacillus megaterium*, Microb. Cell Factories 23 (2024) 35, https://doi.org/10.1186/s12934-024-02304-5.

[41] G. Burra, A.K. Thakur, Unaided trifluoroacetic acid pretreatment solubilizes polyglutamine peptides and retains their biophysical properties of aggregation, Anal. Biochem. 494 (2016) 23–30, https://doi.org/10.1016/j.ab.2015.10.006.

[42] S.-C. Jao, K. Ma, J. Talafous, R. Orlando, M.G. Zagorski, Trifluoroacetic acid pretreatment reproducibly disaggregates the amyloid β-peptide, Amyloid 4 (1997) 240–252, https://doi.org/10.3109/13506129709003835.

[43] J.J. Katz, Anhydrous trifluoroacetic acid as a solvent for proteins, Nature 174 (1954) 509, https://doi.org/10.1038/174509a0.

[44] N.J. Greenfield, Using circular dichroism spectra to estimate protein secondary structure, Nat. Protoc. 1 (2006) 2876–2890, https://doi.org/10.1038/nprot.2006.202.

[45] C.G. Copeland, B.E. Bell, C.D. Christensen, R.V. Lewis, Development of a process for the spinning of synthetic spider silk, ACS Biomater. Sci. Eng. 1 (2015) 577–584, https://doi.org/10.1021/acsbiomaterials.5b00092.

[46] A.E. Albertson, F. Teule, W. Weber, J.L. Yarger, R.V. Lewis, Effects of different post-spin stretching conditions on the mechanical properties of synthetic spider silk fibers, J. Mech. Behav. Biomed. Mater. 29 (2014) 225–234, https://doi.org/10.1016/j.jmbbm.2013.09.002.

[47] G. Zhou, Z. Shao, D.P. Knight, J. Yan, X. Chen, Silk fibers extruded artificially from aqueous solutions of regenerated *Bombyx mori* silk fibroin are tougher than their natural counterparts, Adv Mater 21 (2009) 366–370, https://doi.org/10.1002/adma.200800582.

[48] D. Stengel, J.B. Addison, D. Onofrei, N.U. Huynh, G. Youssef, G.P. Holland, Hydration-induced β-sheet crosslinking of α-helical-rich spider prey-wrapping silk, Adv. Funct. Mater. 31 (2021) 2007161, https://doi.org/10.1002/adfm.202007161.

[49] S. Frische, A.B. Maunsbach, F. Vollrath, Elongate cavities and skin–core structure in *Nephila* spider silk observed by electron microscopy, J Microsc 189 (1998) 64–70, https://doi.org/10.1046/j.1365-2818.1998.00285.x.

[50] B. An, M.B. Hinman, G.P. Holland, J.L. Yarger, R.V. Lewis, Inducing β-sheets formation in synthetic spider silk fibers by aqueous post-spin stretching, Biomacromolecules 12 (2011) 2375–2381, https://doi.org/10.1021/bm200463e.

[51] M. Boulet-Audet, F. Vollrath, C. Holland, Identification and classification of silks using infrared spectroscopy, J. Exp. Biol. 218 (2015) 3138–3149, https://doi.org/10.1242/jeb.128306.

[52] X. Hu, D. Kaplan, P. Cebe, Determining beta-sheet crystallinity in fibrous proteins by thermal analysis and infrared spectroscopy, Macromolecules 39 (2006) 6161–6170, https://doi.org/10.1021/ma0610109.

[53] Q. Wang, P. McArdle, S.L. Wang, R.L. Wilmington, Z. Xing, A. Greenwood, M. L. Cotten, M.M. Qazilbash, H.C. Schniepp, Protein secondary structure in spider silk nanofibrils, Nat. Commun. 13 (2022) 4329, https://doi.org/10.1038/s41467-022-31883-3.

[54] H. Lu, K. Xia, M. Jian, X. Liang, Z. Yin, M. Zhang, H. Wang, H. Wang, S. Li, Y. Zhang, Mechanically Reinforced Silkworm Silk Fiber by Hot Stretching, vol.

2022, Research (Wash D C), 2022 9854063, https://doi.org/10.34133/2022/9854063.
[55] F. Paquet-Mercier, T. Lefèvre, M. Auger, M. Pézolet, Evidence by infrared spectroscopy of the presence of two types of β-sheets in major ampullate spider silk and silkworm silk, Soft Matter 9 (2013) 208–215, https://doi.org/10.1039/C2SM26657A.
[56] A. Huot, T. Lefèvre, J.-F. Rioux-Dubé, F. Paquet-Mercier, A.-P. Nault, M. Auger, M. Pézolet, Effect of mechanical deformation on the structure of regenerated *Bombyx mori* silk fibroin films as revealed using Raman and infrared spectroscopy, Appl. Spectrosc. 69 (2015) 689–698, https://doi.org/10.1366/14-07776.
[57] M. Puerta, M.C. Arango, N. Jaramillo-Quiceno, C. Álvarez-López, A. Restrepo-Osorio, Influence of ethanol post-treatments on the properties of silk protein materials, SN Appl. Sci. 1 (2019) 1443, https://doi.org/10.1007/s42452-019-1486-0.
[58] B. Addison, D. Onofrei, D. Stengel, B. Blass, B. Brenneman, J. Ayon, G.P. Holland, Spider prey-wrapping silk is an alpha-helical coiled-coil/beta-sheet hybrid nanofiber, Chem. Commun. 54 (2018) 10746–10749, https://doi.org/10.1039/c8cc05246h.
[59] J.O. Wolff, M. Rezac, T. Krejci, S.N. Gorb, Hunting with sticky tape: functional shift in silk glands of araneophagous ground spiders (Gnaphosidae), J. Exp. Biol. 220 (2017) 2250–2259, https://doi.org/10.1242/jeb.154682.
[60] T. Köhler, F. Vollrath, Thread biomechanics in the 2 orb-weaving spiders *Araneus diadematus* (araneae, Araneidae) and *Uloborus walckenaerius* (Araneae, Uloboridae), J. Exp. Zool. 271 (1995) 1–17, https://doi.org/10.1002/jez.1402710102.
[61] A. Sensenig, I. Agnarsson, T.A. Blackledge, Behavioural and biomaterial coevolution in spider orb webs, J. Evol. Biol. 23 (2010) 1839–1856, https://doi.org/10.1111/j.1420-9101.2010.02048.x.
[62] B.O. Swanson, T.A. Blackledge, C.Y. Hayashi, Spider capture silk: performance implications of variation in an exceptional biomaterial, J Exp Zool A Ecol Genet Physiol. 307 (2007) 654–666, https://doi.org/10.1002/jez.420.
[63] F. Roloff, S. Strauss, P.M. Vogt, G. Bicker, C. Radtke, Spider silk as guiding biomaterial for human model neurons, BioMed Res. Int. 2014 (2014) 906819, https://doi.org/10.1155/2014/906819.
[64] Y. Dou, Z.P. Wang, W. He, T. Jia, Z. Liu, P. Sun, K. Wen, E. Gao, X. Zhou, X. Hu, J. Li, S. Fang, D. Qian, Z. Liu, Artificial spider silk from ion-doped and twisted core-sheath hydrogel fibres, Nat. Commun. 10 (2019) 5293, https://doi.org/10.1038/s41467-019-13257-4.